Received January 2000
Revised June 2000
Accepted June 2000

Numerical analysis of a primary surface trapezoidal cross wavy duct

Esa Utriainen and Bengt Sundén
Division of Heat Transfer, Lund Institute of Technology, Lund, Sweden

Keywords *Numerical analysis, Hydraulics, Heat transfer, Heat exchangers*

Abstract *A three-dimensional numerical study was conducted to assess the hydraulic and heat transfer performance of a primary surface type heat exchanger surface, called the trapezoidal cross wavy (TCW) duct. This duct is similar to the ducts being used in compact recuperators manufactured by Solar Turbines Inc. The governing equations, i.e. the mass conservation equation, Navier-Stokes equations and the energy equation, are solved numerically by a finite volume method for boundary fitted coordinates. Periodic boundary conditions are imposed in the main flow direction. In this particular case laminar convective flow and heat transfer prevail. Owing to the complex geometry a complicated secondary flow pattern appears in the cross-sectional planes. Details of the recuperator ducts and the numerical method, as well as relevant results, are presented. The overall results are also compared with corresponding results (i.e. Nu numbers, friction factors) of straight ducts with various cross-sectional shapes.*

Nomenclature

A = amplitude of waviness
A_{flow} = area of flow
A_c = area of grid cell face [m^2]
A_{ht} = wall heat transfer area [m^2]
A_k = total wall cross-section area for longitudinal conduction [m^2]
Cmin = minimum of $C = \dot{m}*c_p$ (cold side) and $C = \dot{m}*c_p$ (hot side) [W K^{-1}]
c_p = specific heat of fluid [J kg^{-1} K^{-1}]
D_h = hydraulic diameter of duct [m]
f = fanning friction factor
H = height of top or bottom half of the TCW duct (see Figure 1) [m]
K = coefficient of inclination of straight line
L = length of one module of the TCW duct [m]
L_c = total fluid flow (core) length on one side of an exchanger [m]
$\dot{m}$ = mass flow rate of fluid [kg s^{-1}]
Nu = Nusselt number
p = static pressure [Pa]
p^* = periodic pressure [Pa]
q_w = heat flux from wall [W m^{-2}]
R = radius of circle [m]
Re = Reynolds number
R^2 = correlation coefficient, sum of squares due to regression/sum of squares about mean
S = circumferential length [m]
T = temperature [K]
T^* = periodic temperature [K]
TCW = trapezoidal cross wavy duct (see Figure 1)
Ui = velocities using tensor notation [m s^{-1}]
$\dot{v}$ = volume flow rate [m^3 s^{-1}]
W = velocity in the flow direction (z-direction) [m s^{-1}]
$\overline{w}$ = mass averaged velocity in the flow direction (z-direction) [m s^{-1}]
x_i = coordinate directions using tensor notation [m]
x,y,z = coordinates in the Cartesian system

Greek symbols
α = heat transfer coefficient [W m^{-2} K^{-1}]
β = inclination angle of wall [°]
$\delta_{\alpha\beta}$ = Kronecker's delta, equal to 1 when $\alpha = \beta$, otherwise 0
Δp = pressure loss in duct [Pa]
λ = thermal conductivity [W m^{-1} K^{-1}]
μ = dynamic viscosity [kg m^{-1} s^{-1}]
ρ = density of fluid [kg m^{-3}]

Subscripts
b = bulk of the duct
w = wall

International Journal of Numerical Methods for Heat & Fluid Flow, Vol. 10 No. 6, 2000, pp. 634-648.

Introduction

The application of recuperators in advanced thermodynamic cycles is growing due to stronger demands of low emissions of pollutants and the necessity of improving the cycle efficiency of power plants to reduce the fuel consumption. The requirements on recuperators may be summarized as: high effectiveness and low pressure losses, minimum volume and weight, high reliability and low cost, etc. (see Utriainen and Sundén (1998) or Utriainen and Sundén (2000)).

Present manufacturing techniques provide the means of designing very compact recuperator cores, having hydraulic diameters in the order of one millimeter. Very compact plate-fin type surfaces are presented by Kays and London (1984), for example, and a primary surface type core is presented by Parsons (1985).

Because the density and thermal conductivity of gases are both much lower than those of liquids, gas heat transfer is poor. When a gas is used as the working medium, an enhancement technique may be used to increase the heat transfer coefficient and to reduce the physical size of the recuperator core. Both active and passive heat transfer enhancement techniques are summarized in Webb (1994) and Jacobi and Shah (1995). Active techniques require external power for surface vibration, generation of electric or acoustic fields, etc. Passive techniques include extended surface geometries such as surface protrusions and fins which create local flow structures (secondary flows). Instead of using extended surfaces, the duct geometry may be shaped in a manner so that the insulating near wall thermal and flow layers will be disturbed by secondary flow structures and thus the heat transfer from the gas to the wall will be improved.

Surface protrusion vortex generators like delta winglet pairs have been investigated by Tiggelbeck *et al.* (1994). Their study, for developing duct flow, shows that the average Nu number at an Re number of about 2,000, is increased by 46 percent while the accompanying increase of the friction factor is 177 percent. These dimensionless numbers were compared to the corresponding values of a channel without vortex generators.

An experimental study presented by Olsson and Sundén (1996) investigated thermal and hydrodynamical performance of flat, dimpled and rib-roughened tubes. They concluded that their results are representative for fully developed thermal conditions. Their results show that for Reynolds number, about 1,000, compared to a smooth flat tube, the average Nu number is enhanced by about 50 percent and the friction factor is increased by about 200 percent. Cross-corrugated (CC) ducts have been investigated, both experimentally and numerically, by Ciofalo *et al.* (1996a, 1996b) and Stasiek *et al.* (1996). Their results are interesting for a configuration called CP/UP2, which consists of two metal sheets with different geometrical duct shapes. However, the hydraulic diameter of their duct is defined in a special manner, making direct comparison of Nusselt number and friction factor difficult.

The few examples above from the literature show that enhancing the heat transfer often results in an unacceptably high pressure drop penalty. The plate-fin

type and primary surface type of geometries exhibit promising performance properties. In the primary surface geometry the performance gain is achieved by generation of secondary flows through designing complex geometrical duct shapes.

The simple wavy trapezoidal duct geometry has been investigated by Asako *et al.* (1996); according to the authors of that paper the waviness enhances the convective heat transfer, at Re = 1,616, by 470 percent with an accompanying threefold increase of the friction factor, compared to a straight trapezoidal duct.

The trapezoidal cross wavy (TCW) duct presented in this paper is somewhat similar to the CC duct, the difference being that an additional waviness is introduced in the flow direction (see Figure 1). Also, the TCW duct concept is similar to the primary surface duct concept in a recuperator manufactured by Solar Turbines Inc. (see Parsons (1985)). All simulations in this paper have been performed for laminar flow situations because an investigation of real recuperators showed that, with the operating mass flow rates and the small hydraulic diameters, the Reynolds number is usually less than 2,000. Thus laminar flow prevails.

Governing equations

The Reynolds numbers (Re) considered in this study range from 450 to 2,100. This is a typical Re range for real recuperators, as explained in the previous section.

The methodology of introducing periodic boundaries for solving fully developed flows (see Patankar *et al.*, 1977), is applied in the equations below. Partial periodic boundary conditions are used in the flow direction, taking into account the pressure drop due to wall friction and the temperature increase due to heating by adding extra source terms into the momentum and the temperature equations.

The following equations are valid for an incompressible fluid with constant properties at steady state.

The equation of continuity:

$$\frac{\partial U_i}{\partial x_i} = 0. \tag{1}$$

The Navier-Stokes equation:

$$\frac{\partial}{\partial x_j}\left(\rho \cdot U_j \cdot U_i\right) = -\frac{\partial p^*}{\partial x_i} + \frac{\partial}{\partial x_j}\left[\mu\left(\frac{\partial U_i}{\partial x_j} + \frac{\partial U_j}{\partial x_i}\right)\right] + \beta \cdot \delta_{3i} \tag{2}$$

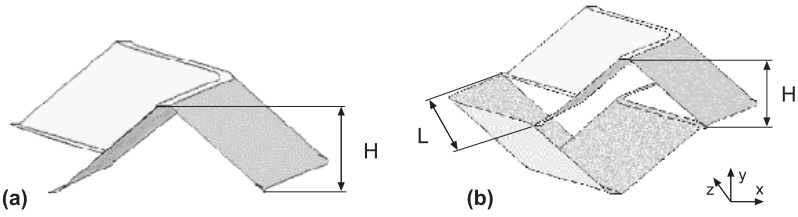

Figure 1.
(a) Simple trapezoidal wavy duct; (b) the TCW duct

where the extra source term, assuming linear pressure drop characteristics in the flow direction is:

$$\beta = \frac{\partial \mathrm{p}}{\partial \mathrm{x_i}}. \tag{3}$$

The pressure p is written as:

$$p = p^* - \beta \cdot z. \tag{4}$$

The pressure p^* behaves periodically and gives no net contribution to the pressure drop over a repeated unit cell.

The temperature equation is:

$$\frac{\partial}{\partial x_j}\left(\rho \cdot U_j \cdot T^*\right) = \frac{\partial}{\partial x_j}\left(\frac{\lambda}{c_p}\frac{\partial T^*}{\partial x_j}\right) - \rho \cdot U_j \cdot \sigma \cdot \delta_{3j} \tag{5}$$

where σ in the extra source term equals:

$$\sigma = \frac{\partial \mathrm{T_b}}{\partial \mathrm{z}} = \frac{\mathrm{q_w} \cdot \mathrm{A_{ht}}}{\underline{\mathrm{m}} \cdot \mathrm{c_p} \cdot \mathrm{L}}. \tag{6}$$

The temperature T is written as:

$$T = T^* + \sigma \cdot z. \tag{7}$$

For prediction of the friction factor f and the Nu number, the following relations were used.

Fanning friction factor:

$$f = \frac{\beta \cdot D_h}{2 \cdot \rho \cdot \bar{W}^2}. \tag{8}$$

The average Nusselt number for a cross-section in a unit cell is calculated from:

$$\overline{Nu} = \frac{q_w \cdot D_h}{\lambda \cdot \left(\overline{T_w - T_b}\right)} \tag{9}$$

where the mean wall to bulk temperature difference for a cross section is:

$$\overline{T_w - T_b} = \frac{\int \left(T_w - T_b\right) \cdot dA_c}{\int dA_c} \tag{10}$$

and the mass averaged bulk temperature is computed from:

$$\mathrm{T_b} = \frac{\int \mathrm{T} \cdot |\mathrm{W}| \cdot \mathrm{dA_c}}{\int |\mathrm{W}| \cdot \mathrm{dA_c}}. \tag{11}$$

The geometry

If two single wavy trapezoidal ducts (see Figure 1a), are brought together with one of them turned 180°, as shown in Figure 1b, the so-called trapezoidal cross wavy (TCW) duct is formed. The TCW duct in Figure 1b is only a representative module formed by corrugated plates in the heat transfer matrix (see Figure 2). The waviness of the duct is composed of circle segments and straight connecting lines. These are described by the relations in Table I, where X1 is the value of x at z = Z1.

The computational domain

The finite volume multiblock method (18 blocks in this study) with a body fitted grid was employed for the computations. The commercially available CFD code CFX 4 from AEA Industrial Technology (1992) has been used for the numerical predictions of the TCW duct performance.

Patankar *et al.* (1977) presented a methodology of periodic boundaries for solving fully developed flows in a module of a periodically repeated waviness of the duct. This methodology is adopted in the present investigation by applying partially periodic boundary conditions in the flow direction (see the governing equations), and fully periodic boundary conditions in the passages between adjacent ducts, perpendicular to the main flow direction, i.e. in the *x* direction (see Figure 3). Figure 3 shows a cut at approximately 1/6L in the duct module in the *z*-direction, which is the main flow direction.

Computational details

In all computations the SIMPLEC algorithm was used for the pressure-velocity coupling. For the velocities U,V and W as well as for the temperature, the

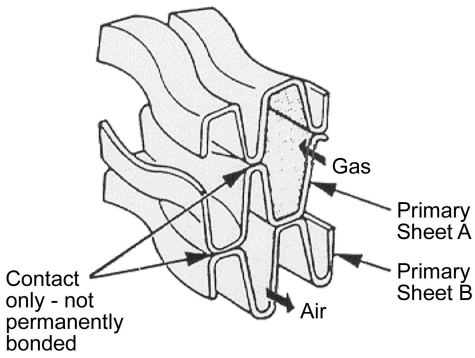

Figure 2.
Primary surface corrugated plates, forming trapezoidal cross wavy ducts

Table I.
Relations describing the waviness of the TCW duct

$0 < z < Z1$	$x = R - ((R)^2 - z^2)^{1/2}$
$Z1 < z < Z2$	$x = X1 + K(z–Z1)$
$Z2 < z < Z3$	$x = R + A\ ((R)^2 - (z–L/2)^2)^{1/2}$
$Z3 < z < Z4$	$x = X1 – K(z–Z4)$
$Z4 < z < Z5$	$x = R - ((R)^2 - (z–Z5)^2)^{1/2}$

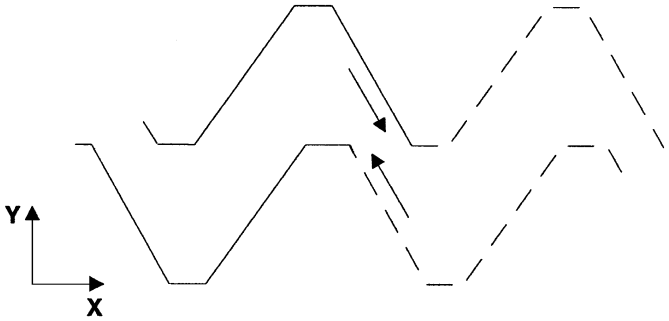

Figure 3.
A cut at a. position 1/6L through the TCW duct in the z-direction

iterative Block Stone's method (solving block by block) was used for solving the equations, and the pressure was solved by the preconditioned conjugate gradient method (ICCG). The default hybrid differencing scheme (HDS) was applied for all variables except for the pressure, where the central differencing scheme (CDS) was used. Under relaxation factors (URF) for the three velocities U, V, W were all equal to 0.65, while for the pressure P and the temperature T URF was unity. No problems in having converged solutions were observed.

Owing to the structured grid design a small displacement is used between the upper and lower halves of the duct geometry, 3-5 percent of the maximum duct width. The wall surfaces created by this displacement are small and should have only a small influence on the average Nu number predicted by the calculations.

The fluid used in the CFD calculations is air with constant properties.

A uniform heat flux, both circumferentially and in the flow direction, is implemented on all walls.

The hydraulic diameter is defined in the conventional manner and is applied in the cut displayed in Figure 2. One has

$$D_h = 4 \cdot \frac{A_{flow}}{S}.$$

This computational approach predicted Nu numbers and *f*-values for straight ducts having rectangular and polygonal cross-sections within 1 percent of the values given in the literature (see Kakac *et al.* (1987)). The accuracy is deemed sufficient.

The effects of heat conduction along the walls are neglected as heat conduction in heat exchangers, according to Shah (1994), has a significant influence only when:

$C=C_{min}/C_{max} \approx 1$, NTU > 10 and $\lambda_c > 0.005$ where:

$$\lambda_c = \frac{\lambda_w A_k}{C_{min} L_c}.$$

The latter criterion should be far from fulfilled as the plate thickness is in the order of 10^{-4}m. The NTU value of 10, for a counter flow recuperator, is only exceeded if the thermal efficiency of the recuperator exceeds 91 percent. Some

heat conduction may also occur in some areas due to local extreme values of the heat transfer coefficient. However, these areas are small compared to the investigated module area and should have a negligible influence on the computed average Nu number.

The Grid

The grids used for the TCW geometries differ due to the structured grid multiblock arrangement, the different geometries of the TCW ducts and also because grid independent solutions are attempted. Table II provides some information on the number of grid points in different directions. Figure 1 shows the coordinate directions, which are used in the computations of the TCW ducts. The structured grid arrangement poses some limitation on the size of the amplitude A of the duct waviness, relative to the width d (see Figure 4). The TCW 5 duct, see Table III, has the largest amplitude A. The grids at the waistline in Figure 4b (between upper and lower halves of the TCW duct) and along the edge in Figure 4a are dense, relative to the rest of the computational domain. This is unfortunate but can only be avoided using an unstructured grid.

The geometrical dimensions of all TCW ducts considered in the computations are listed in Table III. Figure 5 presents the nomenclature of the geometrical variables.

The flow structure in the TCW duct

The flow is a periodic fully developed laminar flow, in the sense that the flow pattern is repeated from module to module, although there are some small changes, e.g. in the flow direction the air side temperature is increasing, the density and pressure are decreasing.

Duct	Direction X	Y	Z	Total
TCW 1	50	50	40	100,000
TCW 2	60	50	45	135,000
TCW 2 test	70	60	50	210,000
TCW 3	61	50	45	137,250
TCW 4	61	50	45	137,250
TCW 4 test	78	60	50	234,000
TCW 5	60	50	45	135,000
TCW 5 test	68	60	45	183,600
TCW 6	60	50	45	135,000
TCW 7	60	50	45	135,000
TCW 8	67	56	40	150080
TCW 9	61	50	45	137250
TCW 10	61	50	45	137250
TCW 11	68	60	45	183,600
TCW 12	68	60	45	183,600
TCW 13	53	50	45	119,250
TCW 14	50	50	45	112,500

Table II.
Number of grid points in computations of the TCW duct

The flow in the near wall region will be disturbed by the secondary flow which results in an increase of velocity- and temperature-gradients and thus enhancement of the heat transfer but also an increase in wall friction and hence pressure drop in these regions.

Secondary flow and isothermal contour plots at different sections

The plots of the secondary flow and isothermal contours are presented at six different sections along the length L of the duct module with the first one at the

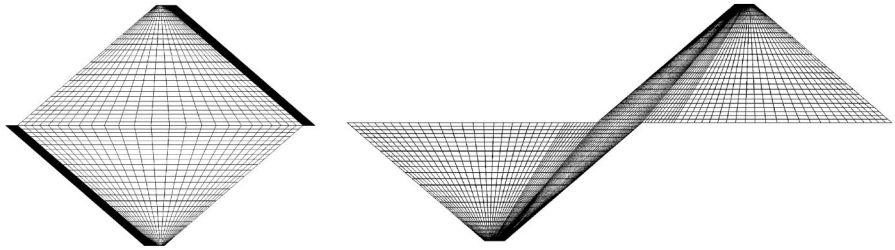

(a) At the beginning of the duct **(b)** At the middle of the duct

Figure 4.
The computational grid of TCW 5

Duct	A/L	H/L	b/L	d/L	c/L	β	R/L
TCW 1	1/30	2/15	1/15	0.2206	1/15	60°	8/15
TCW 2	4/75	2/15	1/15	0.2206	1/15	60°	8/15
TCW 3	4/75	2/15	1/90	0.1651	1/90	60°	8/15
TCW 4	4/75	1/15	1/90	0.1651	1/90	40.9°	8/15
TCW 5	1/15	1/15	1/90	0.1651	1/90	40.9°	8/15
TCW 6	1/15	5/90	1/90	0.1651	1/90	35.8°	8/15
TCW 7	4/75	1/15	1/15	0.2206	1/15	40.9°	8/15
TCW 8	3/35	3/35	1/70	0.2122	1/70	40.9°	24/35
TCW 9	4/75	1/15	1/90	0.1428	1/90	45.3°	8/15
TCW 10	8/75	2/15	1/45	0.2857	1/45	45.3°	8/15
TCW 11	2/15	2/15	1/45	0.3301	1/45	40.9°	8/15
TCW 12	8/75	2/15	1/15	0.2857	1/45	50.6°	8/15
TCW 13	8/75	2/15	2/15	0.3524	2/15	50.6°	8/15
TCW 14	8/75	2/15	4/45	0.3079	2/15	50.6°	8/15

Table III.
Values of geometrical variables used in the computations

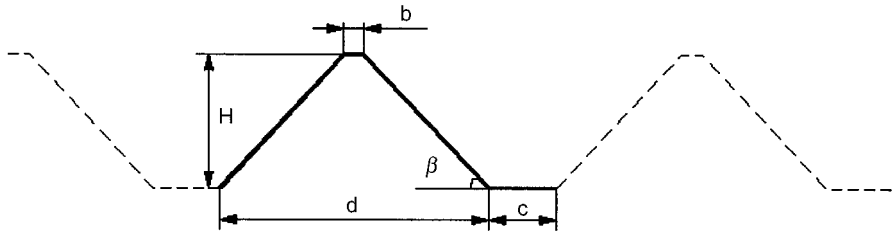

Figure 5.
Geometrical variables of the TCW duct

inlet of the duct module (see Figure 6). Only the top half of the TCW duct is presented in the plots in Figure 7 as the flow structure of the bottom half is identical.

The waviness of the duct together with the inclined walls is favourable for generation of secondary flow structures. The local maximum secondary flow velocities might be as high as 40 percent of the average velocity in the main flow direction in a duct with a high A/L ratio (see Figure 5).

At the section z = 1/6L (see Figure 7), the fluid is leaving the region between the left-hand wall of the top duct half and the right-hand wall of the bottom duct half as these are closing each other. This motion is further enhanced by

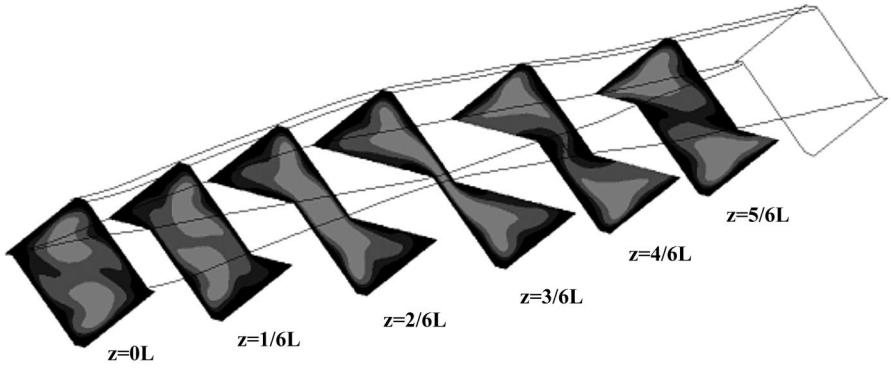

Figure 6.
Positions in z-direction where the secondary flows are presented

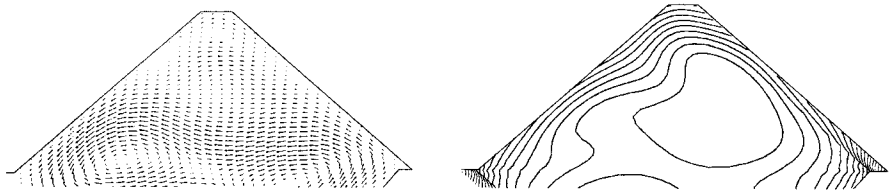

Figure 7a.
Velocity vector plot and isothermal lines at positions z = 0/6L

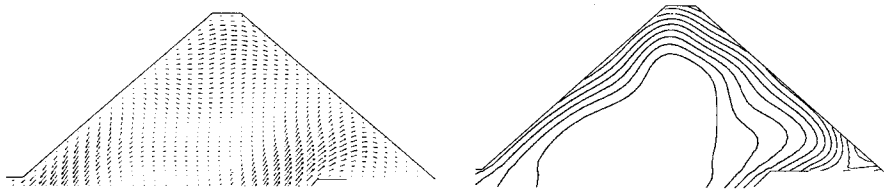

Figure 7b.
Velocity vector plot and isothermal contours at position z = 1/6L

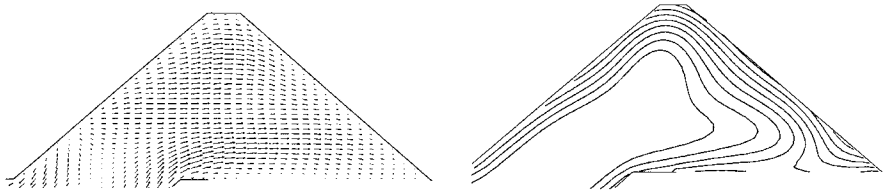

Figure 7c.
Velocity vector plot and isothermal contours at position z = 2/6L

the streamwise flow which is against the walls (top left wall and bottom right wall) at an angle. The direction of the streamwise flow was deflected by the previous streamwise module. The isotherm plot at the same section shows that the top left wall has a temperature close to the bulk temperature, indicating a high local Nu number at the wall. There is no flow through the passage (on the right side) to the adjacent module (in the spanwise direction) as the flow mechanism described above is totally dominating the flow at this section of the TCW duct.

At the section z = 2/6L it can be seen, also at z = 1/6L, that there are some smaller scale vortices close to the top of the duct. Not all of these vortices are rendered in Figure 6 as the secondary flow plots are only a coarse mesh interpolation of the actual dense mesh in Figure 4.

From the section z = 3/6L to section z = 5/6L, when the waviness is shifting back to its original position, the fluid is forced to flow down along the right-hand wall by centrifugal forces acting on the main flow, thus augmenting a large scale flow through the passage to the neighbouring duct (see the arrows in Figure 3). Also a flow appears into the region between the left-hand wall of the top duct half and the right-hand wall of the bottom duct half as the walls are shifting apart.

Isotherm contour plots in the duct show where the wall temperature is close to the main flow bulk temperature, i.e. where the highest Nu numbers can be found as the boundary condition for all walls used in the analysis is a constant wall heat flux.

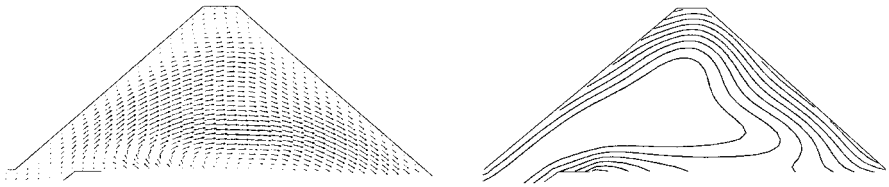

Figure 7d.
Velocity vector plot and isothermal contours at position z = 3/6L

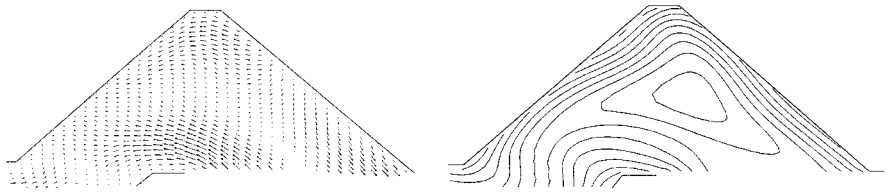

Figure 7e.
Velocity vector plot and isothermal contours at position z = 4/6L

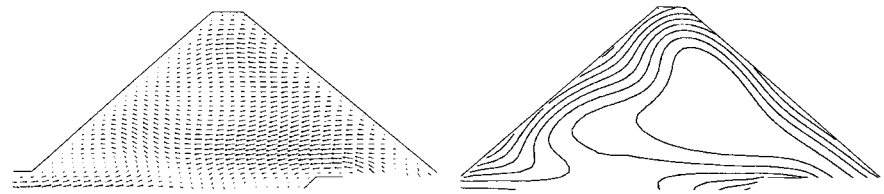

Figure 7f.
Velocity vector plot and isothermal contours at position z = 5/6L

Results of the numerical calculations

The CFD analysis was used for prediction of an average Nu number and an average *f* factor for a module of the TCW duct. The calculations of the TCW duct performance were carried out, assuming laminar flow, up to approximately Re = 2,250.

In both Figures 8 and 9, corresponding results for straight ducts with polygonal and square cross-sections are provided for comparison.

In Figure 8 the average Nu numbers for the different TCW duct configurations are plotted as a function of Re number. It can be seen that the Nu number of a wavy duct is not constant in the laminar flow Re number range, as is the case for laminar flow in straight ducts. The same applies to the product f*Re which also is a function of the Re number for the TCW duct, but for a laminar flow in a straight duct this product, f*Re, is constant (see Figure 9).

Performance comparison of the different geometrical configurations

The most proper way to compare different duct concepts, to be used in a recuperator unit, is to make several complete designs of the unit and compare

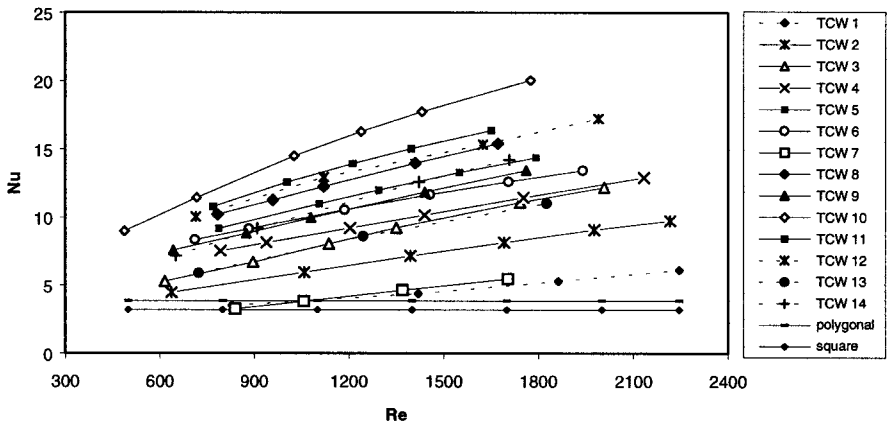

Figure 8.
The Nu number vs. Re number for different TCW configurations

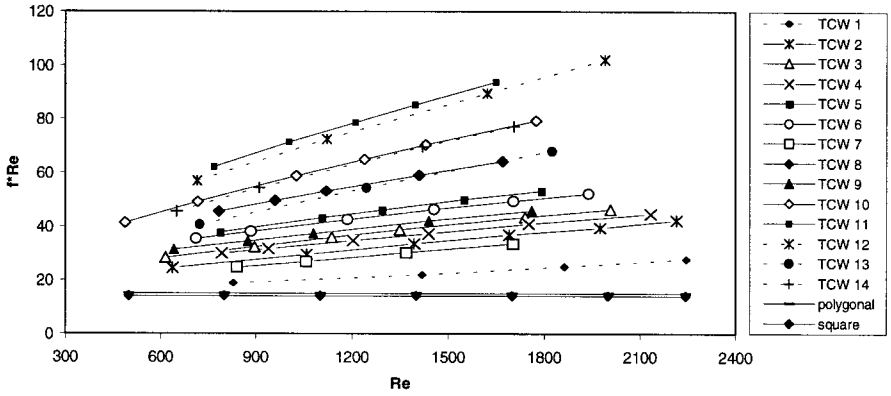

Figure 9.
The product f*Re vs. Re number for different TCW configurations

the performances. As this is a very time-consuming process, a simpler method is adopted for the comparison. In this study the so-called volume goodness criterion is used which, like most other concepts of comparison, only considers the performance on one side of the recuperator, e.g. the gas side. Shah (1978) has presented several other concepts for comparison.

The ducts presented in Figure 10 have equal hydraulic diameter and the Reynolds number ranges from 500 to 2,250. The axes, in Figure 10, represent the heat transfer coefficient (α) and pumping power per unit heat transfer area ($\Delta p \cdot \dot{V}/A_{ht}$), respectively. The results of the TCW ducts are plotted together with those of the reference straight ducts having polygonal and square cross-sections. Values of the *f* factors and Nu numbers for the straight polygonal and square reference ducts have been taken from Kakac *et al.* (1987).

The volume goodness criterion shows that the TCW10 duct concept exhibits the best performance. If one desires to find the optimal (highest for a specified) duct configuration one should try a duct with the A/L ratio approximately 1/10 and with small lengths of the top width b and bottom width c (see Figure 5).

Correlations of the TCW duct results

A least-squares method was employed to fit the TCW data with a power-law function. The TCW 1 duct has been left out from these correlations because the structure of the flow in that duct is not comparable with the other ducts as the amplitude of the waviness is so small that there is no passage between adjacent ducts, in the direction perpendicular to the main flow direction.

The variables included in the correlation are the geometric variables, height of the duct half (H), top width (b), the maximum width of the duct (d), the bottom width (c), maximum amplitude of the waviness (A) and the Reynolds (Re) number. All the variables above are nondimensionalised with the length, in the flow direction, of the duct module (L) (see also Figure 5).

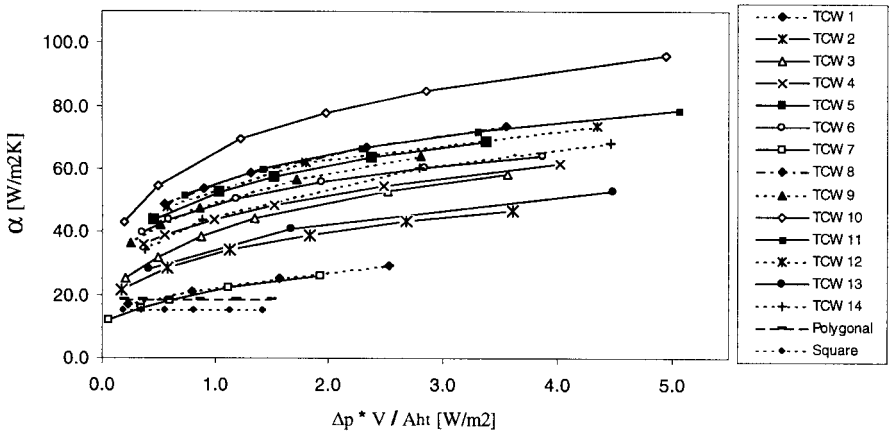

Figure 10.
Volume goodness comparison of the TCW configurations and reference polygonal and square ducts

The correlation of the Nu number predicts all the TCW data within 22.8 percent. The correlation coefficient R^2 for the Nu correlation is 91.7 percent and the standard deviation of log(Nu) is s = 0.0500. The correlation reads:

$$Nu = 1.444\ \mathrm{Re}^{0.622} \left(\frac{A}{L}\right)^{1.63} \left(\frac{b}{L}\right)^{-0.0502} \left(\frac{c}{L}\right)^{0.032} \left(\frac{H}{L}\right)^{0.285} \left(\frac{d}{L}\right)^{-1.47}.$$

The correlation of the f factor predicts all the TCW data within 13.5 percent. The correlation coefficient R^2 for the f correlation is 98.7 percent and the standard deviation of log(f) is s = 0.0197. The correlation reads:

$$f = 33.845\ \mathrm{Re}^{-0.55} \left(\frac{A}{L}\right)^{1.41} \left(\frac{b}{L}\right)^{0.0959} \left(\frac{c}{L}\right)^{-0.0488} \left(\frac{H}{L}\right)^{0.171} \left(\frac{d}{L}\right)^{-0.902}.$$

To illustrate the agreement of these correlations with the numerical results, the correlated values of each simulation are plotted versus the actual results of the numerical calculations (using the code CFX 4) (see Figures 11 and 12).

Final remarks

Numerical prediction of heat transfer and pressure loss properties, using CFD analysis, of a trapezoidal cross wavy (TCW) duct concept is presented. It is shown that the performance of the TCW duct is superior to straight duct configurations. The Nusselt number of the TCW duct is enhanced by up to 400 percent compared to the straight ducts with a similar increase of the pressure drop. In many other enhanced duct concepts the pressure losses are increased more than the heat transfer properties are improved.

The volume goodness graph (see Figure 9) shows that the performance of the TCW ducts varies considerably, with relatively small changes in geometric parameters, and it would therefore be worthwhile to optimise the geometry of the TCW duct if it should be used in a recuperator or other heat exchanger. The amplitude, i.e. the waviness of the duct, is the variable most important for the

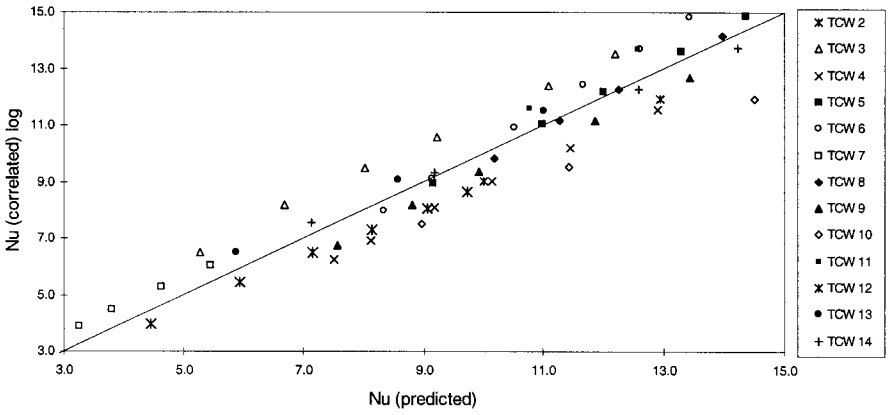

Figure 11.
Correlated Nu numbers vs. predicted Nu numbers for the TCW duct configurations

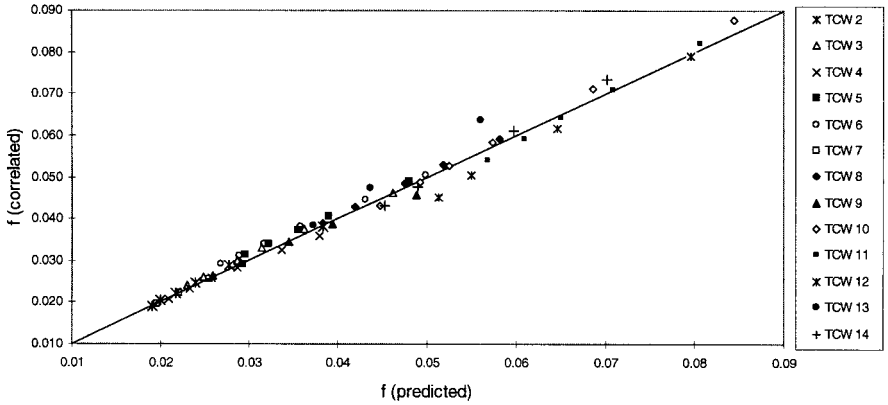

Figure 12.
Correlated *f* factors vs. predicted *f* factors for the TCW duct configurations

enhancement of the heat transfer of the TCW duct concept. This is so because the direction of the main flow is deflected, but also because it opens up the passages to adjacent ducts thus creating large scale secondary flows in the flow domain. The transition from laminar to turbulent flow may be of great importance when a TCW duct should be chosen for a recuperator design. Some of the TCW ducts in the volume goodness graph (see Figure 9) may have transition to turbulence at higher Re numbers than the "optimal" TCW10 duct. As the Nu number is a function of the Re number, the TCW10 duct could be outperformed by another TCW duct with a higher transitional Re number. The pressure drops of both gas and air sides should also be carefully considered in the design process, because these may also influence the choice of duct type.

It was also found that, for laminar flow in the TCW duct, the Nu number and the product f*Re are functions of the Re number, while in straight ducts these are constants (see Figures 7 and 8).

References

AEA Industrial Technology plc (1992), "FLOW 3D user guide", CFD Department, Harwell Laboratory.

Asako, Y., Faghri, M. and Sundén, B. (1996), "Laminar flow and heat transfer characteristics of a wavy duct with a trapezoidal cross-section for heat exchanger application", in Celata, G.P., Di Marco, P. and Mariani, A. (Eds), *2nd European Thermal Sciences and 14th UIT National Heat Transfer Conference 1996*, pp. 1097-104.

Ciofalo, M., Stasiek, J. and Collins, M.W. (1996a), "Investigation of flow and heat transfer in corrugated passages – I. Experimental results", *Int. J. Heat Mass Transfer*, Vol. 39 No. 1, pp. 149-64.

Ciofalo, M., Stasiek, J. and Collins, M.W. (1996b), "Investigation of flow and heat transfer in corrugated passages – II. Numerical simulations", *Int. J. Heat Mass Transfer*, Vol. 39 No. 1, pp. 165-92.

Jacobi, A.M. and Shah, R.K. (1995), "Heat transfer surface enhancement through the use of longitudinal vortices: a review of recent progress", *Exp. Thermal and Fluid Science*, Vol. 11, pp. 295-309.

Kakac, S., Shah, R.K. and Aung, W. (1987), *Handbook of Single-phase Convective Heat Transfer*, John Wiley & Sons, New York, NY.

Kays, W.M. and London, A.L. (1984), *Compact Heat Exchangers*, McGraw-Hill, New York, NY.

Olsson, C.O. and Sundén, B. (1996), "Heat transfer and pressure drop characteristics of ten radiator tubes", *Int. J. Heat Mass Transfer*, Vol. 39, pp. 3211-20.

Parsons, E.L. (1985), "Development, fabrication and application of a primary surface gas turbine recuperator", SAE Technical Paper Series No. 851254.

Patankar, S.V., Liu, C.H. and Sparrow, E.M. (1977), "Fully developed flow and heat transfer in ducts having streamwise-periodic variations of cross-sectional area", *ASME J. Heat Transfer*, Vol. 99, pp. 180-86.

Shah, R.K. (1978), "Compact heat exchanger surface selection methods", *Proc 6th Int. Heat Transfer Conf*., Toronto, Vol. 4, pp. 193-9.

Shah, R.K. (1994), "A review of longitudinal wall heat conduction in recuperators", *J. Energy, Heat and Mass Transfer*, Vol. 16, pp. 15-25.

Tiggelbeck, St., Mitra, N.K. and Fiebig, M. (1994), "Comparison of wing-type vortex generators for heat transfer enhancement in channel flows", *ASME J. Heat Transfer*, Vol. 116, pp. 880-85.

Utriainen, E. and Sundén, B. (1998), "Recuperators in gas turbine systems", ASME paper 98-GT-165.

Utriainen, E. and Sundén, B. (2000), "Recuperators and regenerators in gas turbine systems", *Heat Transfer in Gas Turbine Systems*, WIT Press, Southampton, forthcoming.

Webb, R.L. (1994), *Principles of Enhanced Heat Transfer*, J. Wiley & Sons, New York, NY.

Enter the Emerald Library

Access the MCB University Press online journal collection

Emerald News & Resources

Emerald news, service enhancements, marketing materials, librarian and end-user resources

Alert Service

Join our free alerting service and we'll email contents pages of the journals you select upon publication

Product Information

Detailed information on all Emerald products and services

Subscriber Registration

If you subscribe but have yet to register for online access, go to our subscriber registration page

Free Trials

Take advantage of our free 30 day trial of one or more journals

Help

Contact us with your technical and other customer service queries